Conformational and Vibrational Analysis of Methyl Methanesulfonate, $CH_3SO_2OCH_3$

María E. Tuttolomondo,[†] Amparo Navarro,[‡] Tomás Peña,[‡] Eduardo L. Varetti,[§,||] Stewart F. Parker,[⊥] and Aída Ben Altabef*[,†,||]

INQUINOA, CONICET, Instituto de Química Física, Facultad de Bioquímica, Química y Farmacia, Universidad Nacional de Tucumán, San Lorenzo 456, T4000CAN Tucumán, R. Argentina, Departamento de Química Física y Analítica, Universidad de Jaén, Campus Las Lagunillas, 23071 Jaén, Spain, Centro de Química Inorgánica (CEQUINOR, CONICET-UNLP), Departamento de Química, Facultad de Ciencias Exactas, Universidad Nacional de La Plata, C. Correo 962, 1900 La Plata, R. Argentina, and ISIS Facility, STFC Rutherford Appleton Laboratory, Chilton, Didcot, Oxon OX11 0QX, United Kingdom

Received: April 1, 2009; Revised Manuscript Received: June 5, 2009

The molecular structure of methyl methanesulfonate, $CH_3SO_2OCH_3$, has been optimized by using methods based on density functional theory, coupled cluster, and Moller−Plesset second order perturbation theory (MP2). With regard to $CH_3SO_2OCH_3$, two populated conformations with symmetries C_s and C_1 are obtained, the former being more stable than the latter. The theoretical data indicate that although both *anti* and *gauche* conformers are possible by rotation about the S−O bond, the preferred conformation is *anti*. The total energy as a function of the CSOC dihedral angle has been calculated using the MP2 method with the 6-31G(d) and cc-pVDZ basis sets and the hybrid functional B3LYP using 6-31G(d), 6-311G(d,p), and 6-311++G(d,p) basis sets. A natural bond orbital analysis showed that the lone pair → σ^* hyperconjugative interactions favor the *anti* conformation. Furthermore, the infrared spectra for the liquid and solid phases, the Raman spectrum for the liquid one, and the inelastic neutron scattering spectrum of the solid phase have been recorded, and the observed bands have been assigned to the vibrational modes. The experimental vibrational data, along with calculated theoretical force constants, were used to define a scaled quantum mechanical force field for the target system that enabled us to fit the measured frequencies with a final root-mean-square deviation of 10 cm^{-1}.

1. Introduction

The DNA alkylating agent methyl methanesulfonate (MMS) has been used for years as a DNA damaging agent to induce mutagenesis and in recombination experiments. MMS modifies both guanine (to 7-methylguanine) and adenine (to 3-methyladenine) to cause base mispairing and replication blocking, respectively.[1−3] For that reason, methyl methanesulfonate (MMS), like ethyl methanesulfonate (EMS), has been the subject of many studies since long ago, as was previously commented in the study of EMS.[4]

The aim of the present work is to analyze the molecular structure of MMS and to describe its electronic properties in relation to its action as a potent mutagenic and carcinogenic agent. Thus, the fully optimized geometry was obtained for $CH_3SO_2OCH_3$ using different combinations of theoretical methods and basis sets, and the total energy surface for the torsion angle CSOC was calculated using a variety of computational approaches (both ab initio and density functional theory (DFT)). The study has been completed with a natural bond orbital (NBO)[5] analysis to determine the presence of hyperconjugative interactions, which would favor one conformation over the other. The theoretical structures and conformations of MMS were compared with the experimental and theoretical results previously obtained for $CF_3SO_2OCH_3$,[6] $CF_3SO_2OCF_3$,[7] $CH_3SO_2SCH_3$,[8] and other esters, for all of which the *gauche* conformation is preferred.[6] For MMS, on the contrary, an *anti* conformation is preferred.

In this work we use Bader's atoms in molecules (AIM)[9,10] theory relying on electron density (ρ) to analyze the relative strength of the bonds and subsequent reactivity.

Finally, the infrared, Raman, and inelastic neutron scattering (INS) spectra were recorded and analyzed in order to determine the existence of *gauche* and *anti* conformers in the solid and liquid phases. In addition, the spectral bands were assigned to the different normal modes of vibration of the molecule, and a scaled quantum mechanical (SQM) force field was obtained by means of Pulay's methodology.[11−14]

2. Experimental Section

$CH_3SO_2OCH_3$ (Aldrich Products, Inc.) was used with no further purification and handled with proper protection from atmospheric humidity. The infrared spectra for MMS in the liquid and solid phases were recorded in the 400−4000 cm^{-1} range using a Perkin-Elmer 1600 FTIR instrument. The far-infrared spectrum was obtained with a Bruker IFS 113v FTIR instrument. The spectrum of the solid was obtained after deposition of the substance from a vacuum line onto a KBr window maintained at about 197 K, in a variable temperature cell (RIIC, VLT-2). The Raman spectrum of the liquid at room temperature was obtained with a FRA-106 accessory mounted on a Bruker IFS66 FTIR spectrometer, using 1064 nm light from a Nd/YAG laser for excitation.

* Corresponding author. Tel.: +54 381 431 1044. E-mail address: altabef@fbqf.unt.edu.ar.
[†] Universidad Nacional de Tucumán.
[‡] Universidad de Jaén.
[§] Universidad Nacional de La Plata.
[||] Members of the Carrera del Investigador Científico, CONICET, R. Argentina.
[⊥] STFC Rutherford Appleton Laboratory.

10.1021/jp902993p CCC: $40.75
Published on Web 07/01/2009

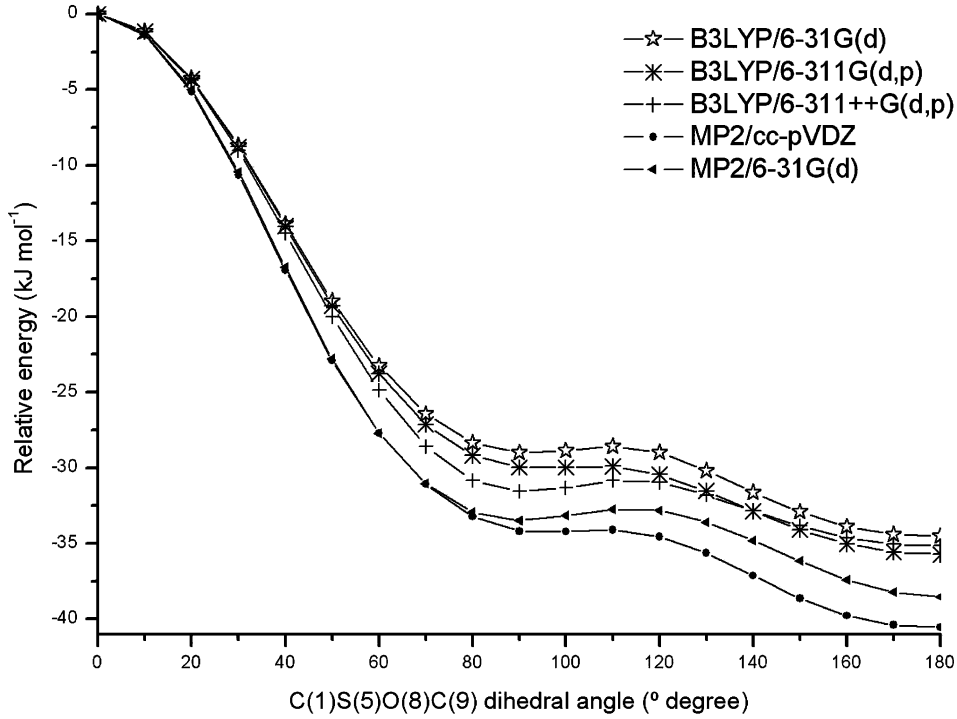

Figure 1. Relative energy of $CH_3SO_2OCH_3$ as a function of the CSOC dihedral angle at different levels of theory.

The INS spectrum was obtained using the time-of-flight spectrometer TOSCA[15] at the ISIS pulsed neutron facility, Rutherford Appleton Laboratory, Chilton, U.K., which has an energy resolution of ~1.25%. The sample was loaded into a thin-walled aluminum sample can and cooled to less than 20 K. Low temperature is required to sharpen the fundamental modes and to diminish the intensity of the phonon wings.

3. Computational Details

The optimized geometry was obtained for $CH_3SO_2OCH_3$ using the density functional theory (DFT) with the B3LYP[16,17] hybrid functional in combination with the standard split-valence basis sets 6-31G(d), 6-311G(d,p), and 6-311++G(d,p). The work by Merz et al.[18] to benchmark the quality of density functional methods in order to reproduce a series of molecular properties shows that B3LYP produces medium quality results on average. The influence of the choice of functional on the optimized geometries as well as on their energies was tested by using the functional mMPW1PW91[19] with the 6-311++G(d,p) basis set. Likewise, the ab initio Moller−Plesset second order perturbations method (MP2), along with the 6-31G(d) and Dunning correlation consistent cc-pVDZ basis sets, was used to optimize molecular structures. Some studies show that the second order perturbations method using correlation consistent basis sets provides energy results of reasonable quality.[18] In addition, the highly correlated method CCSD/cc-pVDZ was employed to achieve the same goals. The conditions of local minima of the total energy surface were assessed by the presence of all real harmonic vibrational frequencies.

The energy surface for the torsion angle CSOC was calculated with the B3LYP/6-31G(d), B3LYP/6-311G(d,p), B3LYP/6-311++G(d,p), MP2/6-31G(d), and MP2/cc-pVDZ methods.

Furthermore, optimization of the most stable conformers was performed by applying the B3LYP method and the 6-31G(d) basis set within the polarizable continuum model (PCM),[20] to take into account the solvent effects on the rotational isomerism.

In order to get insight into the foundations of the relative stability of the two conformers of MMS in the isolated molecule, as well as in different solvents, the natural bond order (NBO) energy decomposition scheme (NBO 4.0 code[21]) was applied at the B3LYP/6-31G(d) level. In addition, an analysis of the reactivity of MMS was done within Bader's atoms in molecules theory (AIM) by using AIM2000 code.[9,10]

All of these methodologies were performed as implemented in the Gaussian 03 package of programs.[22]

The harmonic force field in Cartesian coordinates for $CH_3SO_2OCH_3$ which resulted from the selected DFT procedure was transformed to a set of natural (local symmetry) coordinates through the B matrix[23] obtained with a standard program. The force field obtained was then scaled using the scheme of Pulay et al.;[11−14] i.e., the diagonal force constants are multiplied by scale factors f_i, f_j, ..., and the corresponding interaction constants are multiplied by $(f_i \cdot f_j)^{1/2}$. The scale factors were refined to fit the experimental frequencies. All the vibrational bands were assigned the same weight in the refinement except those with missing or uncertain frequencies which were assigned zero value. No empirical correction of the theoretical geometry was used. The potential energy distribution was subsequently calculated with the resulting SQM force field.

The force field transformation, scaling, and potential energy distribution calculations were performed with the program FCARTP.[24] The atomic displacements, represented graphically by means of the program GaussView,[25] were used to describe the normal modes.

4. Structure and Reactivity Results

4.1. Conformational Analysis. No theoretical and/or experimental structure is available for $CH_3SO_2OCH_3$, and therefore the first goal was to obtain the most stable molecular conformation. A search for secondary minima in the potential energy surface was performed with a series of calculations in which the dihedral CSOC angle was changed in 10° steps and frozen, whereas the rest of the parameters were adjusted using the

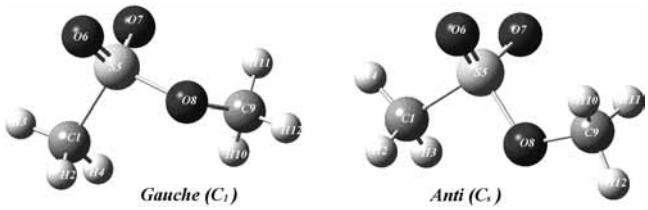

Figure 2. Calculated molecular structure for MMS.

TABLE 1: Energies without ZPE Correction for $CH_3SO_2OCH_3$ at Different Levels of Theory

method	basis	*anti* (C_S) (hartrees)	*gauche* (C_1) (hartrees)	ΔE (*gauche*−*anti*) (kJ mol^{-1})
MP2	6-31G(d)	−702.1875757	−702.1851849	6.27
		−703.6143669	−703.6121883	5.71
B3LYP	6-311G(d,p)	−703.7280135	−703.7266568	3.56
	6-311++G(d,p)	−703.7367787	−703.7346739	5.52
CCSD	cc-pVDZ	−702.2841823	−702.2823153	4.90
MP2		−701.2543485	−701.2518295	6.61

calculation levels mentioned in Computational Details. The results can be seen graphically in Figure 1. The following conformations characterized by local minima were obtained: the *anti* conformer, with lower energy and having C_s symmetry, and the *gauche* conformer with C_1 symmetry, corresponding to two symmetrically equivalent minima which are mirror images (enantiomers). These structures are represented in Figure 2, whereas the numerical results obtained are reported in Table S1 (Supporting Information).

The molecular energies for both conformers calculated at different levels of theory are reported in Table 1. It is observed that the energy of the *anti* conformer is always lower than that for the *gauche* conformer, regardless of the method and basis set used. The prediction of a conformer with a symmetry plane as the most stable one agrees with the results obtained before for the ethyl compound, $CH_3SO_2OCH_2CH_3$.[4] Those are unexpected results when compared with the experimental or theoretical conformations obtained for the related molecules $CF_3SO_2OCH_3$,[6] $CF_3SO_2OCF_3$,[7] $CH_3SO_2SCH_3$,[8] $CCl_3SO_2OCH_2CF_3$,[26] $CF_3SO_2OCH_2CF_3$,[27] and $CF_3SO_2OCH_2CH_3$.[28] In fact, in all these cases a *gauche* conformation with dihedral angles CSOC of 92−115° were found for the most stable structure, and such a conformation was considered a general structural property of covalent sulfonates.[6]

The comparison of calculated molecular geometries among the theoretical methods (Table S1) shows differences that vary from 0.02 Å for the C1−S5 bond with the B3LYP functional to 0.002 Å with MPW1PW91. For O−C bonds, the trend is reversed. The remaining bond distances exhibit differences smaller than 0.02 Å irrespective of the method. As for the bond angles, the largest variation when comparing MP2 and DFT methods is 2.8° for the angle S5−O8−C9. A test of the effect of the basis set size with the B3LYP functional shows differences in bond distances of less than 0.01 Å; for the bond angles the largest differences amount to 1.4° for S5−O8−C9. With regard to the $C_1-S_5-O_8-C_9$ dihedral angle for the C_1 conformer, most of the methods show values within the range 90.0−92.0° except for MP2, which yields values around 94.0°.

4.2. Theoretical Structure in Solution. Table 2 reports the calculated energy differences between both *anti* and *gauche* conformers in several solvents along with their dipole moments. The values in the isolated state have been included for comparative purposes. It is observed that such a difference decreases as the solvent polarity increases, which is the expected behavior since the dipole moment of the *gauche* conformer is larger than that of the *anti* one. Remizov et al.[29] report that the dipole moment of MMS in a CCl_4 ($\varepsilon = 2.63$) solution was 3.75 D, while the calculated ones for the *anti* and *gauche* structures in CCl_4 are 3.61 and 5.31 D, respectively (Table 2). These values confirm that the *anti* form is the predominant one in the low polarity solvent. According to the energy differences of Table 2 and the Boltzmann distribution, the population of the *anti* conformer should be 84% for the isolated molecules, 82% in a CCl_4 solution, and 66% in a $HCCl_3$ solution. These results support the idea that the dipole moment is important in determining the molecular conformation in solution.[30]

TABLE 2: Energy Differences without ZPE Correction and Dipole Moment for $CH_3SO_2OCH_3$ in Different Solvents Calculated with B3LYP/6-31G(d)

	ΔE (kJ mol^{-1})	dipole moment μ (D)	
solvent (ε)	(*gauche*−*anti*)	*anti* (C_s)	*gauche* (C_1)
water (78.39)	1.77	3.85	5.73
acetonitrile (35.9)	1.94	3.83	5.68
acetone (20.7)	2.11	3.79	5.62
chloroform (4.83)	3.33	3.58	5.29
CCl_4 (2.61)	5.31	3.61	5.31
isolated state	5.71	2.98	4.34

4.3. NBO Calculations. In order to get some insight into the intramolecular interactions which justify the relative stability of the *anti* and *gauche* conformers, natural bond orbital (NBO) calculations[5] were made on both forms of MMS. In the NBO analysis, the electronic wavefunction is interpreted as a set of occupied Lewis-type orbitals, paired with a set of formally unoccupied non-Lewis-type orbitals. The electronic interactions within these orbitals, the deviations from the Lewis electronic structure, and the delocalization effects can be interpreted as charge transfers between the filled Lewis orbitals (donors) and the theoretically empty non-Lewis orbitals (acceptors). The stabilization energy of these interactions are mainly of the types lone pair → π^* orbitals (delocalization or mesomeric effect) and lone pair → σ^* orbitals (hyperconjugative effect).

The results of NBO calculations at the B3LYP/6-31G(d) level on the conformers of MMS appear in Table 3. The analysis of the results shows that the delocalization energy does not play a significant role in the relative stabilization of one conformer with respect to the other. The main off-diagonal elements in the Fock matrix correspond to the energy transfer from the lone pairs LPO(8), LPO(6), and LPO(7) to the σ^*C(1)−S(5). It can be seen that for the isolated state and a nonpolar solvent, this stabilizing hyperconjugative effect is higher for the *anti* conformer than for the *gauche* form, but that in aqueous solution these values are reversed. Thus, a decrease in the value of the hyperconjugation is observed as the polarity of the solvent increases. This effect is more pronounced in the *anti* form than in the *gauche* one and results in the inversion of the values in the most polar solvent. Since the most altered off-diagonal components are LPO(8) → σ^* S(5)−O(6) and LPO(8) → σ^* S(5)−O(7), it is suggested that such effect is due to the interactions between these free pairs and the water molecules.

4.4. AIM Calculations. As mentioned in the Introduction, the carcinogenic and mutagenic power of MMS has been extensively studied and also compared with other similar compounds, such as ethyl methanesulfonate (EMS),[4] both being substances which induce mutations by electrophilic attack.

In order to rationalize the alkylating properties of $CH_3SO_2OCH_3$, Bader's atoms in molecules quantum theory (AIM)[9] has been repeatedly shown to be of aid in the characterization of bonds. In the AIM theory, the nature of a

TABLE 3: Important Hyperconjugative Interactions (kJ/mol) and Occupancy of the Natural Bond Orbitals for $CH_3SO_2OCH_3$ Calculated Using the B3LYP/6-31G(d) Method

	anti ϕ			gauche ϕ		
interaction[a]	(CSOC) = 180.0° isolated state	(CSOC) = 180.0° CCl_4 solution	(CSOC) = 180.0° H_2O solution	(CSOC) = 91.78° isolated state	(CSOC) = 92.41° CCl_4 solution	(CSOC) = 90.84° H_2O solution
LPO(8) → σ* C(1)−S(5)	3.72	3.80	3.89	24.66	25.83	26.79
LPO(8) → σ* S(5)−O(6)	34.44	35.07	35.78	21.03	22.44	23.66
LPO(8) → σ* S(5)−O(7)	34.44	35.07	35.78	15.68	15.42	16.26
LPO(6) → σ* C(1)−S(5)	83.43	83.01	82.64	82.39	82.26	82.18
LPO(6) → σ* S(5)−O(8)	138.90	135.09	133.13	141.66	139.94	138.48
LPO(6) → σ* S(5)−O(7)	97.35	97.22	90.79	96.68	95.76	91.17
LPO(7) → σ* C(1)−S(5)	83.43	83.01	82.64	83.60	83.10	82.60
LPO(7) → σ* S(5)−O(8)	138.90	135.09	133.13	136.94	129.16	126.36
LPO(7) → σ* S(5)−O(6)	97.35	97.22	85.27	97.56	100.36	99.78
σ* S(5).O(8) → σ* O(8)−C(9)	15.42	16.68	18.14	19.35	20.90	22.57
total	727.40	721.26	640.84	719.55	715.17	709.85
σ O(8)−C(9)	1.99201	1.99177	1.99150	1.99133	1.99101	1.99069
σ* O(8)−C(9)	0.01107	0.01128	0.01152	0.01275	0.01336	0.01395
d (Å)	1.447	1.450	1.454	1.443	1.448	1.453

[a] LP is a lone pair on the specified atom.

TABLE 4: B3LYP/6-31G(d) Calculated Bond Critical Point (BCP) Data and BCP Distances (in au) to Attractors[a] for $CH_3SO_2OCH_3$

		anti (C_s)							*gauche* (C_1)						
bond (X−Y)[a]		ρ	$\nabla^2\rho$	BCP−X	BCP−Y	*d* (Å)	*q* (X)	*q* (Y)	ρ	$\nabla^2\rho$	BCP−X	BCP−Y	*d* (Å)	*q* (X)	*q* (Y)
C(1)−S(5)	isolated	0.2061	−0.4135	1.502	1.884	1.794	0.021	1.203	0.2035	−0.4000	1.520	1.881	1.800	0.006	1.221
	water	0.2071	−0.4192	1.499	1.879	1.788	0.026	1.199	0.2051	−0.4084	1.515	1.874	1.793	0.105	1.212
S(5)−O(8)	isolated	0.2121	−0.1555	1.236	1.872	1.644	1.203	−0.528	0.2114	−0.1358	1.234	1.871	1.643	1.221	−0.524
	water	0.2150	−0.1092	1.221	1.869	1.634	1.199	−0.527	0.2144	−0.0924	1.220	1.867	1.613	1.212	−0.518
O(8)−C(9)	isolated	0.2294	−0.3240	1.801	0.938	1.447	−0.528	0.318	0.2317	−0.3406	1.794	0.940	1.443	−0.524	0.309
	water	0.2266	−0.3111	1.805	0.943	1.454	−0.527	0.326	0.2284	−0.3511	1.797	0.952	1.453	−0.518	0.315

[a] The first and second atom to the bond CP.

bonding interaction can be determined through an analysis of the properties of the charge density and its Laplacian $\nabla^2\rho$ at the bond critical point (BCP), and by the properties of the atoms, which are obtained by integrating the charge density over the atom. Table 4 presents the bond critical point data for $CH_3SO_2OCH_3$.

It can be seen that the charge density of the O(8)−C(9) bond critical point is relatively high and decreases on going from the isolated state to aqueous solution. The value of charge density in the *anti* conformer is relatively smaller than for the *gauche* conformer. In the S(5)−O(8) vicinal bond the situation is reversed, so in this case this bond experiences an increase in the electronic density when going from the isolated state to the aqueous solution. The distances between bond critical points and attractor are given in Table 4. The length of the O(8)−C(9) bond path increases when going from the isolated state to the aqueous solutions in both conformers. The O(8)−C(9) bond critical point for both conformers is closer to the C(9) atom than to the O(8) atom, which points to a charge transfer from C(9) to O(8) in the bond region (see Table 4 and Figure 3).

Thus, it is observed (Table 4) that the charge of the group $C(9)H_3$ becomes slightly more positive in aqueous solution (0.33 (*anti*); 0.32 (*gauche*)). This feature makes the $-CH_3$ group more reactive in aqueous solutions such as the cellular media.

These results agree with the NBO analysis of the O(8)−C(9) bond since a decrease of the electronic population in the bonding orbital O(8)−C(9) along with an increase in its antibonding counterpart σ*O(8)−C(9) is observed (Table 4), which involves a weakening of the bond.

The results obtained suggest that the MMS molecule in aqueous solution is a more effective electrophilic reagent than in the isolated state.

5. Vibrational Results

The assignment of the experimental bands to the normal modes of vibration of MMS was based on the comparison with related molecules[4,7,8,26−28] and with the results of the calculations performed in this work. The observed far-infrared, INS, and Raman spectra are shown in Figure 4, whereas the infrared spectra of the liquid and solid phases appear in Figure 5. The frequencies of the observed spectral features are collected in Table 5.

The B3LYP calculations reproduced the normal frequencies of vibration of $CH_3SO_2OCH_3$ with the following root-mean-square deviations (rmsd) values for each basis set: 6-31G(d), 75 cm^{-1}; 6-311G(d,p), 62 cm^{-1}; 6-311++G(d,p), 63 cm^{-1}. Although the second and third basis sets reproduce somewhat better the experimental frequencies, the results obtained with the combination B3LYP/6-31G(d) were used for the vibrational analysis, in order to facilitate the comparison of the present results with those obtained previously for related molecules. The frequencies calculated with this method for the 30 normal modes of vibration of the *anti* conformer of $CH_3SO_2OCH_3$ (18 A′ + 12 A″) appear in Table 6 where they are compared with the measured ones.

The vibrational frequencies corresponding to the *gauche* conformer were also calculated and appear in Table S2 as part of the Supporting Information, additional to the present work.

5.1. Infrared Evidence about the Presence of Both Conformers in the Samples. A comparison between the calculated frequencies for the two conformers shows that for several vibrational modes these values differ appreciably. That difference is particularly important for the antisymmetric SO_2 stretching, for which intense bands are predicted at 1367 cm^{-1} (*gauche* conformer) and 1342 cm^{-1} (*anti* conformer), that is,

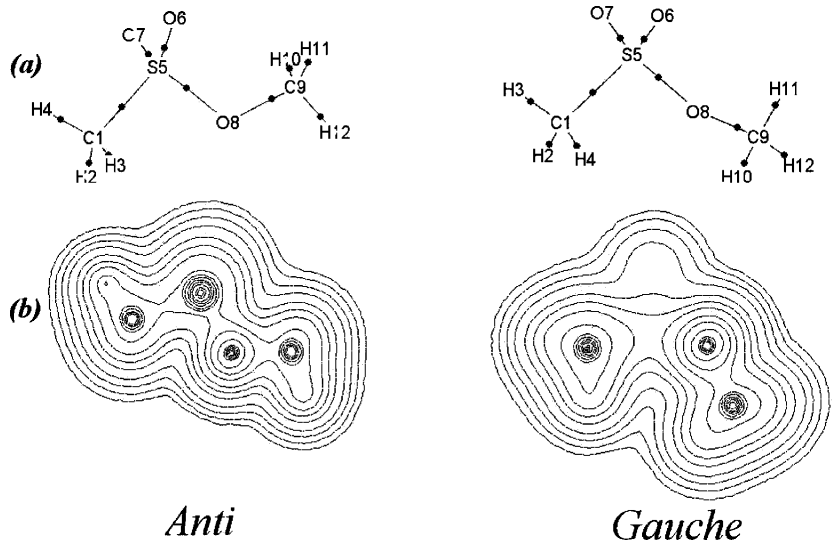

Figure 3. (a) Molecular structure of the *gauche* and *trans* conformers of MMS; nuclei and bond critical points are represented by large and small spheres, respectively. (b) Contour maps of charge density in the C(9)−O(8)−S(5) plane. BCOs are given as triangles.

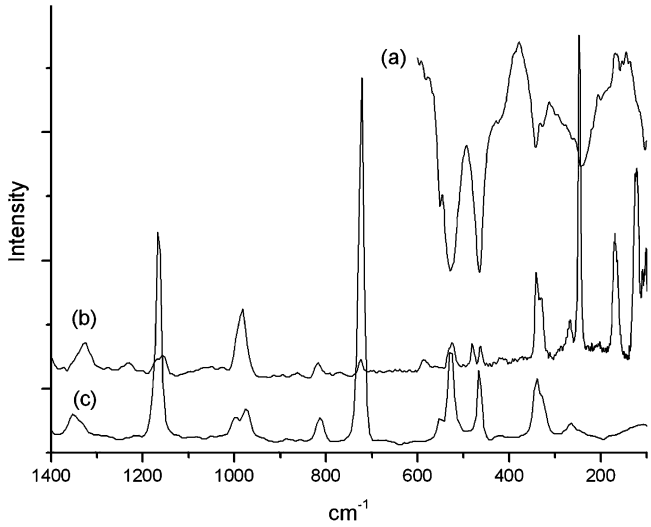

Figure 4. Spectra of MMS: (a) far-infrared spectrum of the liquid at room temperature (resolution 2 cm^{-1}; path length 0.1 mm); (b) INS spectrum of the solid; (c) Raman spectrum of the liquid.

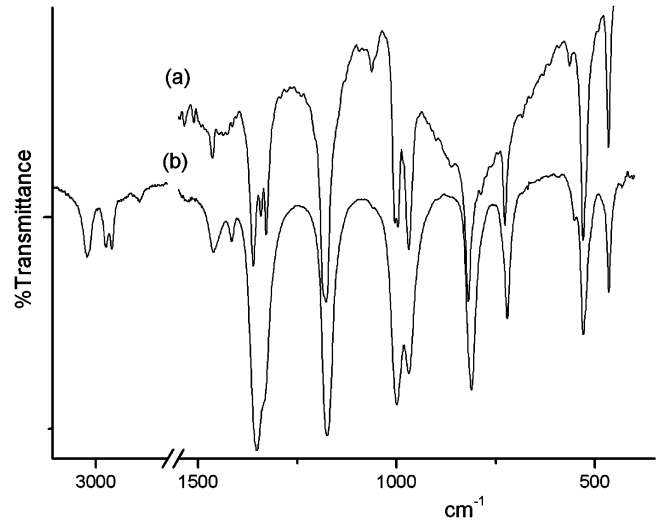

Figure 5. Infrared spectra of MMS: (a) solid phase at low temperature (resolution 2 cm^{-1}; thin layer on KBr window); (b) liquid phase at room temperature (resolution 2 cm^{-1}; path length 0.1 mm).

with a separation of 25 cm^{-1}. In fact, two rather intense bands are observed in the expected region of the infrared spectrum of a solution of MMS in CCl_4 (Figure 6, trace c) at 1371 and 1350 cm^{-1}, with a difference of 21 cm^{-1}. The infrared spectrum of a solution in a polar solvent like CCl_3H ($\mu = 1.01$; Figure 6, trace b) shows still two bands, broadened and now centered at 1361 and 1340 cm^{-1} but accompanied by new weak bands and shoulders. There is a relative increase in the intensity of the first band, assigned to the *gauche* conformer, probably as a consequence of the solvent polarity (see above the discussion about the theoretical structures in solutions). The third spectrum of Figure 6 (trace a) corresponds to the solid substance, where the molecule can be considered immersed in a media of relatively high polarity (MMS molecules have a dipole moment near 3 μ, as shown in Table 2) and therefore subjected to important interactions. The band located at 1329 cm^{-1}, which appears weakly in the other spectra, could be originated by such interactions.

Two bands should also appear for the symmetric SO_2 stretching, calculated at 1156 cm^{-1} for the *gauche* conformer and 1154 cm^{-1} for the *anti* conformer. The corresponding band in the infrared spectrum of the solid appears split in two components centered at 1183 and 1176 cm^{-1} (Table 5), indicating again the presence of both conformers.

The band observed at 466 cm^{-1} in the infrared spectra is assigned to the SO_2 rocking vibrational mode (see below). Such a band appears split in the INS spectrum, with components at 478 and 459 cm^{-1} (Table 5) which are assigned to the *anti* and *gauche* conformers, respectively. These measured values are near the calculated ones, which are 443 and 429 cm^{-1}.

5.2. Assignment of Bands. The assignment of the observed bands to the different modes of molecular vibration should be made before a scaling of the theoretical force field is attempted. The following assignments are based on the comparison with related molecules and on the graphical visualization of the calculated atomic displacements for each theoretical frequency.

5.2.1. Methyl Group Modes. Three clearly defined bands and some shoulders appear in the infrared and Raman spectra of the liquid substance in the 3080−2900 cm^{-1} region, which can be assigned to the expected six CH_3 stretching modes. The two relatively intense bands in the Raman spectrum, located at 2966 and 2943 cm^{-1}, are assigned to the CH_3 symmetric stretching

TABLE 5: Frequencies of Observed Bands in the Infrared, Raman, and INS Spectra of $CH_3SO_2OCH_3$ (Units Are cm^{-1})

infrared[a]		INS	Raman[b]	
liquid	solid	solid	liquid	assignment[c]
3030 w				ν_{as} SCH_3
3026 w			3028 (15)	ν_{as} OCH_3
3009 sh				
2989 sh				
2968 w			2966 (29)	ν_s OCH_3
2946 w			2943 (98)	ν_s SCH_3
2851 vw			2849 (7)	
1461 w	1463 w		1461 (7)	δ_{as} OCH_3
1440 sh			1437 sh	δ_{as} SCH_3
1415 w	1414 w	1417	1417 (12)	δ_s OCH_3
1352 vs	1361 vs (*anti*)	1326	1352 (7)	ν_{as} SO_2
1329 vs (*gauche*)				
1333 sh	1342		1331 sh	δ_s SCH_3
1174 vs	1183 vs (*gauche*)	1172	1179 sh	ν_s SO_2
1176 vs (*anti*)				
1179 sh		1155	1165 (63)	ρ OCH_3
1056 w sh	1063 vw−1052 sh		1050	?
998 s	1004 s		998 (7)	ρ SCH_3
997 s	984 br			
969 s	969 s		974 (9)	ν O−C
812 s	820 s	817	813 (7)	ν C−S
721 m	727 m	722	723 (100)	ν S−O
552 w	564 w		552 (7)	wag SO_2
529 m	530 m	526	528 (26)	δ SO_2
466 m	466 m	478 (*anti*)	465 (21)	ρ SO_2
459 (*gauche*)				
342 m		342	341 (17)	δ CSO
328 w			328 (17)	tw SO_2
262 sh		270	265 (4)	?
242 m		244		δ SOC
200 vw		207		?
180 sh vw		171		τ SCH_3
104 vw			105 (4)	τ OCH_3
82 w				τ S−O

[a] sh, shoulder; br, broad; s, strong; w, weak; m, medium; v, very. [b] Relative band heights in parentheses. [c] ν, stretching; δ, angular deformation; ρ, rocking; wag, wagging; tw, twisting; τ, torsion.

modes. Comparison with CH_3SO_2OH[31] and $CH_3SO_2SCH_3$[8] show that the 2943 cm^{-1} band should be associated with the SCH_3 group, whereas the corresponding CH_3 antisymmetric stretching bands should be strongly overlapped in the broad feature centered at 3030 cm^{-1}. The 2966 cm^{-1} band is therefore assigned to the OCH_3 symmetric stretching modes, with the shoulders located at about 3026 and 3009 cm^{-1} assigned to the corresponding antisymmetric modes; the corresponding bands of $CF_3SO_2OCH_3$ appear at 2980 and 3064 cm^{-1}, respectively.[32]

The CH_3 bending modes should appear in the 1500−1300 cm^{-1} region, which shows several bands and shoulders. The intense band located at 1352 cm^{-1} in that region should be assigned to the SO_2 antisymmetric stretching mode (see section 5.2.2). The shoulder at ca. 1333 cm^{-1} is assigned to the SCH_3 symmetric deformation, located at 1336 in CH_3SO_2OH,[31] whereas the weak shoulders located at ca. 1440 cm^{-1} are assigned to the corresponding antisymmetric deformations; the experimental splitting between symmetric and antisymmetric modes is therefore of ca. 104 cm^{-1}, which can be compared with the 96 cm^{-1} calculated value. A splitting of 31 cm^{-1} is predicted for these modes in the OCH_3 moiety; therefore, the 1415 cm^{-1} band, which is more intense in the Raman and INS spectra, and the 1461 cm^{-1} bands are assigned to the symmetric and antisymmetric deformations of that group.

The calculations show that the methyl rocking modes of the OCH_3 group appear at higher frequencies than those of the SCH_3 moiety. The Raman band located at 1165 cm^{-1}, showing a shoulder at about 1179 cm^{-1} in the liquid infrared spectrum, can be assigned to the OCH_3 rocking modes. In fact, this is a complex spectral region in which the mentioned rocking modes overlap with the SO_2 symmetric stretching features. The INS spectrum shows in that region a broad band with maxima at 1172 and 1155 cm^{-1}. The 998 cm^{-1} band, split in the spectrum of the solid (Table 5), is assigned to the SCH_3 rocking modes. A broad and relatively intense band centered at 984 cm^{-1} appears in this region in the INS spectrum.

5.2.2. SO_2 Group Modes. The SO_2 antisymmetric and symmetric stretching modes appear in the regions 1357−1467 and 1140−1200 cm^{-1}, respectively, in the molecules CY_3SO_2X studied previously.[4,7,8,26−28] Therefore, the bands observed at 1352 and 1174 cm^{-1} in the infrared spectrum of the liquid substance are immediately assigned to those two vibrational modes. These bands appear split in the infrared spectrum of the solid (Table 5) and demonstrate the presence of both conformers in the sample, as discussed before.

The band located at 529 cm^{-1} in the liquid infrared spectra is assigned to the SO_2 bending mode, which appears in the 488−538 cm^{-1} region in the above-mentioned compounds. The three low frequency modes corresponding to the movements of the whole SO_2 group should be now considered. The following assignments are proposed, with the corresponding assignment regions for the above-mentioned molecules in parentheses: SO_2 wagging, 552 cm^{-1} (510−628 cm^{-1}); SO_2 rocking, 466 cm^{-1} (382−463 cm^{-1}); SO_2 twisting, 328 cm^{-1} (310−351 cm^{-1}). These assignments are also supported by the calculations.

5.2.3. The Skeletal Modes. The 969 cm^{-1} band is assigned to the C−O stretching mode, as suggested by the calculations. With the same argument the 812 cm^{-1} band is assigned to the S−C stretch, which appears at 816 cm^{-1} in $CH_3SO_2OCH_2CH_3$.[4] The band located at 721 cm^{-1} is assigned to the S−O stretch, which is found at 733 cm^{-1} in that molecule.

The medium intensity band observed at 342 cm^{-1} in the infrared spectrum is assigned to the CSO bend, a vibrational mode which appears at 338 cm^{-1} in $CH_3SO_2OCH_2CH_3$.[4] The irregular band centered at 242 cm^{-1} corresponds to a mode which has the SOC bend as the main contributor, according to the calculations.

5.2.4. The Torsional Modes. Three weak and ill-defined low frequency bands located at 180, 104, and 82 cm^{-1} are tentatively assigned to the torsional modes, as appear in Tables 5 and 6.

5.3. Calculation of Force Constants. The vibrational analysis and force field calculation were performed only for the most stable *anti* conformer of $CH_3SO_2OCH_3$.

The force field in Cartesian coordinates, as generated by the Gaussian code, was transformed to the set of nonredundant, natural coordinates defined in Table S3 (Supporting Information), which take into account the local symmetry around the C, S, and O atoms. The resulting force constants were subsequently scaled according to the methodology described in the Computational Details. A set of initial scale factors was defined for some coordinates using values recommended by Kalincsák and Pongor[14] and using unity for the rest; these scale factors were subsequently refined by a nonlinear least-squares procedure in order to fit the experimental frequencies. The initial and final values appear in Table S4.

The calculated frequencies, rmsd final value, and potential energy distribution are given in Table 6. It can be seen that most of the vibrational modes have a participation of ≥70% of one defined coordinate, whereas other modes represent very complex vibrations where several coordinates are heavily involved.

TABLE 6: Observed and Calculated Frequencies (in cm^{-1}), Infrared and Raman Intensities, and Potential Energy Distribution for the *Anti* Conformer of $CH_3SO_2OCH_3$

mode	observed	calculated[a]	calcd SQM [b]	IR intensities[c]	Raman activity[d]	potential energy distribution (≥10%)[e]	approximate description of mode
A′							
ν_1	3030	3196	3032	0.1	65.1	100 S_1	ν_{as} SCH_3
ν_2	3026	3184	3022	9.3	81.8	95 S_2	ν_{as} OCH_3
ν_3	2943	3097	2966	0.0	100.5	100 S_3	ν_s SCH_3
ν_4	2966	3073	2942	28.0	97.8	95 S_4	ν_s OCH_3
ν_5	1461	1534	1482	11.1	12.9	95 S_5	δ_{as} OCH_3
ν_6	1440	1489	1436	7.1	13.8	92 S_6	δ_{as} SCH_3
ν_7	1415	1483	1414	0.6	2.6	100 S_7	δ_s OCH_3
ν_8	1333	1387	1339	12.1	0.5	100 S_8	δ_s SCH_3
ν_9	1179	1202	1169	1.6	4.8	91 S_9	ρ OCH_3
ν_{10}	1174	1154	1164	142.2	8.2	72 S_{10} + 16 S_{24}	ν_s SO_2
ν_{11}	969	1033	969	99.2	3.6	71 S_{11} + 18 S_{12} + 19 S_{13}	ν C−O
ν_{12}	998	999	978	169.8	3.3	77 S_{12}	ρ SCH_3
ν_{13}	812	782	818	102.6	5.9	56 S_{13} + 19 S_{15}	ν S−C
ν_{14}	721	686	714	88.3	21.7	72 S_{14}	ν S−O
ν_{15}	552	521	558	23.4	10.0	30 S_{13} + 40 S_{15} + 13 S_{18}	wag SO_2
ν_{16}	529	480	519	13.8	4.4	88 S_{16}	δ SO_2
ν_{17}	342	326	350	8.7	1.9	30 S_{15} + 48 S_{17} + 25 S_{18}	δ CSO
ν_{18}	242	211	228	11.7	10.0	69 S_{17} + 53 S_{18}	δ SOC
A″							
ν_{19}	3030	3207	3042	0.0	54.8	100 S_{19}	ν_{as} SCH_3
ν_{20}	3009	3155	2993	13.0	39.5	100 S_{20}	ν_{as} OCH_3
ν_{21}	1461	1514	1462	5.0	16.0	93 S_{21}	δ_{as} OCH_3
ν_{22}	1440	1483	1431	3.5	16.2	92 S_{22}	δ_{as} SCH_3
ν_{23}	1352	1342	1352	227	3.4	93 S_{23}	ν_{as} SO_2
ν_{24}	1179	1184	1195	13.4	3.5	68 S_{24} + 13 S_{10}	ρ OCH_3
ν_{25}	998	1004	998	1.04	6.6	27 S_{11}+ 51 S_{25}	ρ SCH_3
ν_{26}	466	443	481	13.9	1.7	72 S_{26} + 11 S_{27}	ρ SO_2
ν_{27}	328	292	316	1.2	1.7	26 S_{26} + 87 S_{27}	tw SO_2
ν_{28}	180	193	164	0.1	0.0	100 S_{28}	τ SCH_3
ν_{29}	104	140	121	0.4	0.2	100 S_{29}	τ OCH_3
ν_{30}	82	45	76	6.8	0.5	100 S_{30}	τ S−O
rmsd (cm^{-1})	75		10				

[a] B3LYP/ 6-31G(d) calculation. Observed and calculated values in cm^{-1}. [b] From scaled quantum mechanics force field (see text). [c] Units are km mol^{-1}. [d] Units are $Å^4/(amu)^{-1}$. [e] Numbers correspond to coordinates as defined in Table S2.

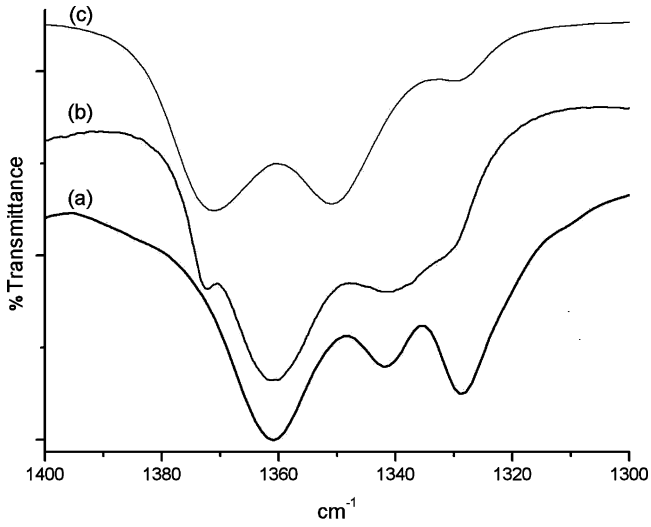

Figure 6. Infrared spectra of MMS in the SO_2 antisymmetric stretching region: (a) solid state; (b) CCl_3H solution; (c) CCl_4 solution.

The SQM force field (Table S5) was used to calculate the internal force constants appearing in Table 7, which are compared with the equivalent values of $CH_3SO_2OCH_2CH_3$[4] and $CF_3SO_2OCH_3$.[28]

6. Conclusions

The optimized molecular geometry and conformation for methyl methanesulfonate, $CH_3SO_2OCH_3$, were calculated using MP2 and DFT techniques and different basis sets. The structural results showed that the *anti* conformation, having a plane of symmetry, is the most stable one. Natural bond orbital calculations were performed in order to justify the preferred conformation of the molecule. Infrared, Raman, and inelastic neutron scattering spectra were obtained for methyl methanesulfonate, in which the bands assignable to the 30 normal modes of vibration were observed. The presence of the two conformers

TABLE 7: Force Constants in Internal (Valence) Coordinates for *anti*-$CH_3SO_2OCH_3$ and Related Molecules

force constant[a]	CH_3SO_2 OCH_3[b]	$CH_3SO_2OCH_2$ CH_3[c]	CH_3SO_2 OH[c]	CF_3SO_2 OCH_3[d]
f(C−H) (SCH_3)	4.90	4.96	4.91	−
f(C−H) (OCH_3)	4.88	4.90		5.07
f(C−S)	3.52	3.74	3.47	3.15
f(S−O)	4.27	4.08	4.31	5.03
f(S═O)	9.77	9.82	10.2	10.53
f(C−O)	4.27	4.13	−	4.50
f(O═S═O)	1.34	1.26	1.35	1.17
f(O−S═O)	1.39	1.31	1.41	1.37
f(C−S−O)	1.37	1.29	1.31	1.14
f(C−S═O)	1.17	1.10	1.21	1.03
f(O−C−H)	0.68	0.68	−	0.73
f(H−C−H)	0.43−0.48	0.43−0.45	0.42	0.47
f(S−O−C)	1.14	0.833	−	1.16
f(S═O/S═O)	0.0026	0.0035		−0.073
f(C−H/C−H)	0.020	0.027		0.029

[a] Units are mdyn $Å^{-1}$ for stretchings and stretch/stretch interactions and mdyn Å rad^{-2} for angular deformations. [b] This work. [c] Reference 4. [d] Referenece 28.

in the samples of the substance was evidenced by the splitting of several vibrational bands, in correspondence with the frequency values predicted by the calculations for each conformer. The theoretical force field obtained for the *anti* conformer was scaled in order to reproduce as well as possible the experimental frequencies. The resulting SQM force field served to calculate the potential energy distribution, which revealed the physical nature of the molecular vibrations, and the force constants in internal coordinates, which could be compared to the values obtained before for related chemical species.

Acknowledgment. The research grants provided by CONICET (Consejo Nacional de Investigaciones Científicas y Técnicas, PIP 5633-2005), ANPCyT (Agencia Nacional de Promoción Científica y Tecnológica, PICT 11127-2002), and UNLP (Universidad Nacional de La Plata) are gratefully acknowledged, as well as the financial help received from CIUNT (Consejo de Investigaciones de la Universidad Nacional de Tucumán). The STFC Rutherford Appleton Laboratory is thanked for the provision of neutron beam facilities.

Supporting Information Available: Geometry calculations at different levels of theory (Table S1), frequencies and intensities calculated for the *gauche* conformer (Table S2), definitions of the local symmetry coordinates (Table S3), scaling factors for force constants (Table S4), and SQM force field matrix (Table S5). This material is available free of charge via the Internet at http://pubs.acs.org.

References and Notes

(1) Wulff, B. B. H.; Thomas, C. M.; Parniske, M.; Jones, J. D. G. *Genetics* **2004**, *167*, 459.
(2) Li, W. *J. Chromatogr., A* **2004**, *1046*, 297.
(3) Sega, G. A. *Mutat. Res.* **2004**, *134*, 113.
(4) Tuttolomondo, M. E.; Navarro, A.; Peña, T.; Varetti, E. L.; Ben Altabef, A. *J. Phys. Chem. A* **2005**, *109*, 7946.
(5) Reed, A. E.; Curtiss, L. A.; Weinhold, F. *Chem. Rev.* **1988**, *88*, 899.
(6) Trautner, F.; Ben Altabef, A.; Fernández, L. E.; Varetti, E. L.; Oberhammer, H. *Inorg. Chem.* **1999**, *38*, 3051.
(7) Tuttolomondo, M. E.; Argañaraz, P. E.; Varetti, E. L.; Hayes, S. A.; Wann, D. A.; Robertson, H. E.; Rankin, D. W. H.; Ben Altabef, A. *Eur. J. Inorg. Chem.* **2007**, 1381.
(8) Tuttolomondo, M. E.; Navarro, A.; Peña, T, P. E.; Varetti, E. L.; Hayes, S. A.; Wann, D. A.; Robertson, H. E.; Rankin, D. W. H.; Ben Altabef, A. *J. Phys. Chem. A* **2007**, *111*, 9952.
(9) Bader, R. F. W. *Atoms in Molecules, A Quantum Theory*; Claredon Press: Oxford, 1990.
(10) Biegler-Köning, F.; Schönbohm, J.; Bayles, D. AIM2000: A Program to Analyze and Visualize Atoms in Molecules. *J. Comput. Chem.* **2001**, *22*, 545.
(11) Pulay, P.; Fogarasi, G.; Pongor, G.; Boggs, J. E.; Vargha, A. *J. Am. Chem. Soc.* **1983**, *105*, 7037.
(12) Rauhut, G.; Pulay, P. *J. Phys. Chem.* **1995**, *99*, 3093.
(13) Rauhut, G.; Pulay, P. *J. Phys. Chem.* **1995**, *99*, 14572.
(14) Kalincsák, F.; Pongor, G. *Spectrochim. Acta A* **2002**, *58*, 999.
(15) Colognesi, D.; Celli, M.; Cilloco, F.; Newport, R. J.; Parker, S. F.; Rossi-Albertini, V.; Sacchetti, F.; Tomkinson, J.; Zoppi, M. *Appl. Phys. A* **2002**, *74 [Suppl.]*, S64–S66.
(16) Becke, A. D. *J. Chem. Phys.* **1993**, *98*, 5648.
(17) Lee, C.; Yang, W.; Parr, R. G. *Phys. Rev.* **1988**, *B37*, 785.
(18) Hehre, W. J.; Radom, L.; Scheleyer, P. V. R.; Pople, J. A. *Ab Initio Molecular Orbital Theory*; Wiley: New York, 1986.
(19) Adamo, C.; Barone, V. *J. Chem. Phys.* **1998**, *108*, 664.
(20) Miertus, S.; Scrocco, E.; Tomasi, J. *Chem. Phys.* **1981**, *55*, 117.
(21) Gledening, E. D.; Badenhoop, J. K.; Reed, A. D.; Carpenter, J. E.; Weinhold, F. F. Theoretical Chemistry Institute, University of Wisconsin: Madison, WI, 1996.
(22) Frisch, M. J.; et al. *GAUSSIAN 98*, revision A.7; Gaussian, Inc.: Pittsburgh, PA, 1998.
(23) Wilson, E. B.; Decius, J. C.; Cross, P. C. *Molecular Vibrations*; McGraw-Hill: New York, 1955.
(24) Collier, W. B. *Program FCARTP (QCPE # 631)*; Department of Chemistry, Oral Roberts University: Tulsa, OK, 1992.
(25) Nielsen, A. B.; Holder, A. J. *GaussView, User's Reference*; Gaussian, Inc.: Pittsburgh, PA, 1997−1998.
(26) Tuttolomondo, M. E.; Navarro, A.; Varetti, E. L.; Ben Altabef, A. *Spectrochim. Acta* **2005**, *61*, 1011.
(27) Tuttolomondo, M. E.; Fernández, L. E.; Navarro, A.; Varetti, E. L.; Ben Altabef, A. *Spectrochim. Acta* **2004**, *60A*, 611.
(28) Tuttolomondo, M. E.; Navarro, A.; Varetti, E. L.; Ben Altabef, A. *J. Raman Spectrosc.* **2005**, *36*, 427–434.
(29) Remizov, A. B.; Butenko, G. G. *J. Appl. Spectrosc.* **1974**, *20* (3), 418–420.
(30) Bond, D.; Schleyer, P. v. R. *J. Org. Chem.* **1990**, *55*, 1003–1013.
(31) Durig, J. R.; Zhou, L.; Schwartz, T.; Gounev, T. J. *J. Raman Spectrosc.* **2000**, *31*, 193.
(32) Fernández, L. E.; Ben Altabef, A.; Varetti, E. L. *Spectrochim. Acta* **1996**, *52A*, 287.

JP902993P